Heliyon 9 (2023) e20924

Contents lists available at ScienceDirect

Heliyon

journal homepage: www.cell.com/heliyon

Synthesis and physicochemical characterization of mesoporous hydroxyapatite and its application in toothpaste formulation

Azarmidokht Nikfallah [a,c], Ali Mohammadi [b,c], Mohammadsadegh Ahmadakhondi [d,e], Mehdi Ansari [f,*]

[a] Department of Pharmaceutics, Faculty of Pharmacy, Damghan Branch, Islamic Azad University, Damghan, Iran
[b] Department of Drug and Food Control, Faculty of Pharmacy, Tehran University of Medical Sciences, Tehran, Iran
[c] Pharmaceutical Quality Assurance Research Center, The Institute of Pharmaceutical Sciences (TIPS), Tehran University of Medical Sciences, Tehran, Iran
[d] Department of Orthodontics, School of Dentistry, Tehran University of Medical Sciences. Tehran, Iran
[e] Dental Research Center of Dentistry, Dentistry Research Institute, Tehran University of Medical Sciences, Tehran, Iran
[f] Department of Drug and Food Control, Faculty of Pharmacy, Kerman University of Medical Sciences, Kerman, Iran

ARTICLE INFO

Keywords:
Hydroxyapatite
Mesoporous
Physicochemical properties
Toothpaste
Formulation
Thymol
Dentistry
Prevention

ABSTRACT

The key characteristics of mesoporous hydroxyapatite, such as high porosity and expansive surface area, along with its biocompatibility with dental tissues and potential as a delivery vehicle for active ingredients, have recently garnered significant research focus. In the present study, mesoporous hydroxyapatite was synthesized using a precipitation technique and was subsequently characterized via X-ray diffraction, Fourier transform infrared, dynamic light scattering, field emission scanning electron microscopy and N_2 adsorption–desorption isotherms. The results revealed that the synthesized mesopore particles exhibited significant adsorption potential, and were thereby considered a carrier of thymol, an effective antibacterial on oral pathogens. Specifically, mesoporous hydroxyapatite's surface area and pore volume were approximately 2.66-fold and 1.95-fold higher than hydroxyapatite's. A statistically significant divergence in the release profiles of thymol from thymol-loaded mesoporous hydroxyapatite and thymol-loaded hydroxyapatite was noted, as indicated by the similarity factor ($f_2 < 50$). Evaluation of organoleptic parameters (taste, odor, smoothness, appearance) showed that thymol-loaded mesoporous hydroxyapatite toothpaste had superior organoleptic attributes compared to thymol-loaded hydroxyapatite toothpaste. However, both formulations were acceptable regarding pH and stability and were desirable regarding abrasiveness with no significant difference compared to the standard formulation ($p > 0.05$). Overall, the findings demonstrate the suitability of mesoporous hydroxyapatite as an abrasive material for developing hydroxyapatite-based toothpaste formulations.

1. Introduction

Toothpaste is a dentifrice that is used to remove dental plaque and maintain oral hygiene or as a delivery system for therapeutic agents [1], mainly fluorides [2] and antimicrobials [3]. Common abrasive components in toothpastes include calcium carbonate,

* Corresponding author
E-mail address: mansari@kmu.ac.ir (M. Ansari).

https://doi.org/10.1016/j.heliyon.2023.e20924
Received 16 March 2023; Received in revised form 25 September 2023; Accepted 11 October 2023
Available online 12 October 2023

Abbreviations

mHA	mesoporous hydroxyapatite
HA	hydroxyapatite
XRD	X-ray diffraction
FTIR	Fourier transform infrared
DLS	dynamic light scattering
FESEM	Field Emission Scanning Electron microscopy
mHA@thymol	thymol-loaded mHA
HA@thymol	thymol loaded HA
SLS	sodium lauryl sulfate
HPMC	hydroxypropyl methylcellulose
Na CMC	sodium carboxymethyl cellulose
EDX	energy-dispersive X-ray
BET	Brunauer-Emmett-Teller
BJH	Barrett-Joyner-Halenda
PBS	phosphate buffered saline
IUPAC	International Union of Pure and Applied Chemistry

sodium bicarbonate, hydrated silica, and dicalcium phosphate, which are typically used at concentrations ranging from 10 % to 40 % w/w [4,5]. These abrasive agents in the toothpaste formulations are crucial in teeth whitening but can also have detrimental effects. Excessive abrasiveness in toothpaste may increase surface roughness and lead to a loss in the structural integrity of the teeth due to a decrease in mineral content [6,7]. Therefore, further research is needed to *develop abrasives* with effective cleaning capabilities that minimize harm to teeth [6].

Hydroxyapatite (HA) is a stable, non-toxic [8], and biocompatible ceramic: its chemical formulation is $(Ca)_{10}(PO_4)_6(OH)_2$. HA serves as the primary mineral component of dental enamel and dentine. Due to these benefits, HA is widely used in dentistry for applications such as tooth remineralization, reduction of tooth sensitivity, oral biofilm control, and tooth whitening [9]. Additionally, HA showed promising results for Molar Incisor Hypomineralisation (MIH) treatment [10] and remineralization of early dental caries [11]. Various HA-formulated oral care products like dentifrice, toothpaste, mouthwashes, and gels are available [12].

Recently, mesoporous materials have garnered interest for their high surface areas, large and adjustable pore size, and substantial pore volumes, properties that make them ideal for developing new catalysts, adsorbents, and drug delivery systems [13,14]. Combining the advantage of HA and mesoporous material can lead to enhanced properties [9,14]. Several techniques have been successfully employed to form HA structures, such as sol-gel approaches, precipitation, hydrothermal processes, microemulsion, and electrodeposition techniques [15]. Among them, precipitation is a standard method for HA production under controllable laboratory conditions [16].

Natural antibacterial ingredients in toothpastes are gaining popularity as well [17]. Thymol, a phenolic compound, has shown significant antibacterial and antifungal activities against oral pathogens and is a common active ingredient in dental formulations like mouthwashes, tooth gels, and varnishes [18–20]. The volatility, reactivity, and pungent odor of thymol are mitigated when loaded onto porous cellulose and mesoporous silica carriers [21–24].

Limited studies have examined the adsorptive systems used in toothpaste formulations, explicitly focusing on the potential of mesoporous hydroxyapatite (mHA) as an abrasive with versatile applications. In the current experiment, mHA was successfully synthesized, featuring a mesoporous structure with a high surface area. Thymol was selected for a comparative study of mHA and HA adsorptive properties, an area not sufficiently studied in previous investigations. Due to the biocompatibility, high surface area and high pore volume of mHA, the development of toothpaste formulations using mHA as a multi-purpose abrasive shows promising prospects for oral health care products.

2. Materials and methods

Calcium acetate, sodium bicarbonate, ethylene glycol, disodium hydrogen phosphate, methanol, absolute ethanol (99.8 %), glycerin, sodium lauryl sulfate (SLS), sodium saccharin, sodium fluoride, and sodium hydroxide were obtained from Merck, Germany. Meanwhile, HA, thymol, Carbopol® 940, hydroxypropyl methylcellulose (HPMC), sodium carboxymethyl cellulose (Na CMC), and Sorbitol 70 % were purchased from Sigma-Aldrich, USA. Zahra Rosewater Company, Iran, generously provided peppermint oil. All chemicals were of analytical grade and used without further purification. Deionized water was used for all experiments.

2.1. Synthesis of mHA nanostructures

The hollow mHA nanostructures were synthesized using a modified procedure from previous work [25]. An aqueous solution (100 mL) of 0.31 M calcium acetate was combined with a 1 M sodium bicarbonate aqueous solution and 1000 mL ethylene glycol. The resulting mixture was stirred for 3 h at room temperature. Disodium hydrogen phosphate aqueous solution (0.25 M) was subsequently

added. The final mixture was stirred for an additional hour at room temperature, allowing the mHA nanostructure to form after 24 h at 60 °C. The synthesized nanostructure was collected through centrifugation, washed with absolute ethanol and deionized water, and dried at 60 °C.

2.2. Characterization

A range of analytical techniques were employed to comprehensively characterize and differentiate the synthesized mHA from commercially obtained HA. Given the availability of specific instrumentation and insights from relevant literature, the techniques selected for this study included Fourier Transform Infrared Spectroscopy (FTIR), Field Emission Scanning Electron Microscopy (FESEM) coupled with Energy-Dispersive X-ray Spectroscopy (EDX), Dynamic Light Scattering (DLS), Brunauer-Emmett-Teller (BET) and X-Ray Diffraction (XRD).

FTIR spectra were acquired with Thermo Avatar® through a wave number range of 4000–400 cm^{-1} using the KBr disc method in the solid state for structure analysis. This technique was utilized to examine the interactions between mHA and thymol and elucidate the samples' structural attributes. Specific attention was paid to functional groups; changes such as intensification, elimination, or addition of peaks were markers for assessing interactions.

The mHA, HA and mHA@thymol morphology was assessed using FESEM (Zeiss Sigma 300®, Germany). Comparisons were made by observing micrographs of similar scales. EDX analysis provided map of elemental composition, allowing us to determine elemental distribution within the synthesized product. Samples were affixed to double-sided carbon tapes on stainless steel stubs and coated with an ultra-thin gold layer (1.5–3.0 nm).

DLS was conducted at 25 °C by use of Malvern Zetasizer Nano Series (Worcestershire, UK) to measure the average particle size of dispersed samples (mHA and HA) in water. This method was primarily employed to gauge the average particle sizes of the dispersed samples, irrespective of their cohesion. Complementary FESEM imaging was also employed to confirm whether DLS-measured sizes represented actual particle dimensions.

Employing the BET method, we characterized the samples' specific surface area and pore size distribution. BET is considered the most direct method for surface area measurements and, by extension, offers insights into the adsorption properties of the mesoporous particles involved. The specific surface area and pore size distribution were analyzed using N_2 adsorption/desorption isotherms (Besorp mini II, Bel, Japan) at 77° K utilizing BET and Barrett-Joyner-Halenda (BJH) models, respectively. Measurements were conducted with a known mass of the solid sample in powder form after degassing at 100 °C.

Crystallography and phase analysis were performed using XRD peaks (Philips pw 1730) with Cu Kα radiation ($\lambda = 0.1540$ nm) over a scanning interval (2θ) range from 5.49° to 79.99°. Interpreting XRD peaks and comparing them with the standard cards allow for characterization of the components.

2.3. Loading of thymol onto mHA

A stock solution of thymol in methanol (1000 mg L^{-1}) was prepared. Sequentially, standard solutions of 100, 150, and 200 mg L^{-1} thymol were prepared by dilution with water. Thymol was loaded onto mHA and HA by adding 20 mL of each standard solution to varying quantities of mHA and HA (20 mg, 50 mg, and 100 mg). Samples (2 mL) were taken at specific intervals and replaced with fresh solvent. The adsorbed thymol quantities were measured at predetermined time intervals using a UV-VIS spectrophotometer (T80 PG instruments, England) at a wavelength of 276 nm. The optimized loaded nanoparticles were calculated using Equation (1):

$$Q_t = \frac{(C_0 - C_t) \times V}{m} \quad (1)$$

In this equation, Q_t represents the amount of thymol adsorbed onto mHA particles (μg mg-1), m denotes the mass of mHA particles (mg), C_0 and C_t signify the initial and final thymol concentrations (obtained via UV- adsorption spectrophotometer), respectively. V is the volume of thymol solution [25]. The optimized thymol-loaded mHA (mHA@thymol) and thymol-loaded HA (HA@thymol) were used for subsequent release studies.

2.4. In vitro thymol release profile

The release profile of thymol was ascertained using a Franz vertical diffusion cell (Ashke-Shisheh Co., Iran). A pre-soaked cellulose membrane separated the upper and lower sections of the diffusion cell. In each receptor compartment, 30 mL of Phosphate buffered saline (PBS) with a pH of 7.4 served as the dissolution medium. The temperature was consistently held at 37 °C ± 0.5 °C while the media in the receptor compartment was stirred at 450 rpm. The mHA@thymol suspension (0.5 mL containing 2.4 mg of mHA@thymol acquired during the loading stage) was added to the donor compartment. Samples with 2 mL volume were withdrawn from the receptor chamber at pre-defined time points over 6 h (0.25, 0.5, 1.0,1.5, 2.0, 3.0, 4.0, 5.0, and 6.0 h points), and immediately replaced with an equal volume of preheated fresh PBS at 37 °C ± 0.5 °C. Samples were then analyzed using UV–Vis spectroscopy at a wavelength of 276 nm, and the cumulative thymol release was calculated based on a standard curve. Release profiles of HA@thymol and the control (thymol solution) were also determined and compared using the similarity factor (f_2) as described by Equation (2):

$$f_2 = 50 \times \log\left[\left(1 + \left(\frac{1}{n}\right)\sum (R_t - T_t)^2\right)^{-0.5} \times 100\right] \quad (2)$$

In this equation, n signifies the time points for the calculation. R_t and T_t denote the ratio of thymol released from the comparator and the test suspension at the time t, respectively. A resulting f_2 value of 50 or greater indicates a similar release profile of the compared components [26].

2.5. Formulation of toothpaste

The process for formulating mHA@thymol and HA@thymol toothpastes was carried out in a step-by-step manner, as detailed below.

2.5.1. Preparation of mHA@thymol

Thymol was dissolved in 5 mL of absolute ethanol, to which mHA was added. The solution was thoroughly mixed and subsequently kept at 35 °C for 2 h to allow complete solvent evaporation. The same steps were repeated to prepare HA@thymol.

This study included thymol in the toothpaste formulation at a concentration of 0.5 % w/w, as corroborated by previous studies investigating thymol's antibacterial efficacy against oral pathogens [27].

2.5.2. Preparation of toothpaste formulation

The thickening agents were amalgamated separately with deionized water and subjected to continuous stirring to form mucilage. Sorbitol and glycerin were then incrementally added to this mucilage, accompanied by constant mixing. A separate liquid phase was formulated by transferring Sodium saccharin and sodium fluoride to the remaining formulation water and combining them. This surfactant phase was then slowly integrated into the mucilage above using continuous stirring, resulting in a smooth paste. mHA loaded with thymol was then blended into this mixture. At the final stage, peppermint oil was incorporated, and stirring was maintained until a homogenous paste was achieved. The preparation of the HA@thymol toothpaste followed an identical procedure [28]. The ingredients of the toothpaste formulations are detailed in Table 1.

2.6. Evaluation of toothpaste organoleptic and physicochemical properties

2.6.1. Organoleptic properties

The organoleptic characteristics (i.e., color, taste, odor, texture) was assessed via sensory evaluation. Fifteen pharmacy students voluntarily participated in this study section and provided written informed consent prior to their involvement. Before the assessment, the participants were educated on the specific organoleptic parameters under investigation-namely, uniformity, smoothness, taste, odor, spreadability, and dryness. Subsequently, a brief structured questionnaire was administered to the participants to assess each of the specified organoleptic parameters qualitatively, and the participants were asked to rate each on a scale ranging from '-' indicating a negative trait to '+++' denoting a highly positive characteristic. The collected questionnaire responses have been compiled and are presented in Table 4. To provide clarity on the chosen organoleptic metrics, their operational definitions are as follows:

Texture Indicators: Spreadability, uniformity, and smoothness were selected as signifiers of the texture of formulations. Uniformity is considered a measure of the consistency and homogeneity of the formulations. Smoothness assesses the presence of rough or palpable particles within the formulation. Spreadability was evaluated explicitly by observing the formulation's behavior when spread on a glass surface.

Table 1
Composition of toothpaste formulations: Ingredients and quantities utilized.

	Formulation Number	
Constituent (%)	1	2
mHA	10.0	0.0
HA	0.0	10.0
Carbopol 940	0.5	0.5
HPMC	5.0	5.0
CMC Na	5.0	5.0
Sorbitol 70 %	30.0	30.0
Glycerin	4.0	4.0
SLS	1.5	1.5
Thymol	0.5	0.5
sodium fluoride	0.1	0.1
Peppermint oil	0.1	0.1
Sodium Saccharin	0.1	0.1
All except water	56.8	56.8
Water	43.2	43.2
Total	100.0	100.0

Odor and Taste: For assessing both odor and taste, volunteers were asked to evaluate the overall acceptability of the formulations' smell and flavor.

2.6.2. pH measurement

Toothpaste samples were dissolved in deionized water to measure the pH, following the ISO11609 standard [29]. The dilution ratio was set at 1:3, and pH readings were taken using an 827 pH lab instrument from Metrohm, Switzerland.

2.6.3. Dentine and enamel abrasion

Sample preparation for dentin and enamel abrasion tests conformed to the ISO11609 standard, employing a specialized brushing machine (V8 cross brushing machine, Oaj Andishan Spadan Co., Isfahan, Iran). Surface roughness measurements, denoted as nominal

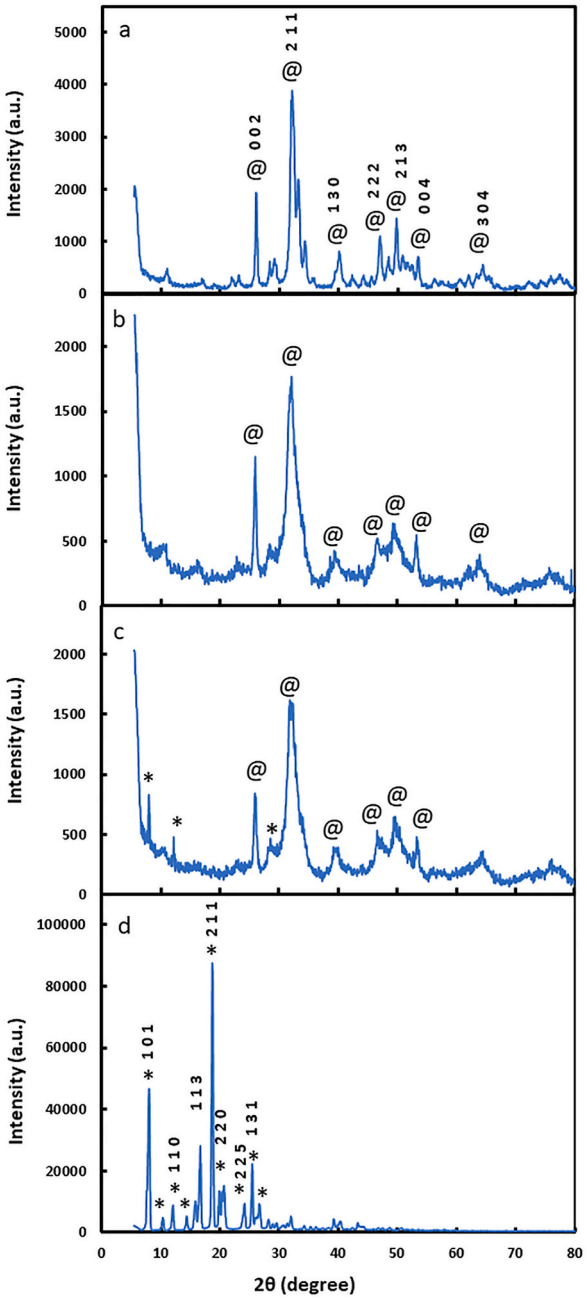

Fig. 1. X-ray Diffraction (XRD) patterns of a) HA b) mHA c) mHA@thymol d) thymol.
HA: hydroxyapatite; mHA: mesoporous hydroxyapatite; mHA@thymol: thymol-loaded mHA.

Ra values, were conducted for each experimental interval. Comparative analysis between experimental groups utilized an independent *t*-test via Microsoft Excel 2019. Specifically, the roughness levels of F_1 and F_2 formulations were compared and juxtaposed with a standard formulation. A p-value less than 0.05 was considered statistically significant.

3. Results and discussion

3.1. The synthesized and compounded HA characterization

The synthesis of mHA in this study was validated through comprehensive characterization. A notable constraint of the method detailed in section 2.1 is the limited yield of mHA; however, scaling the process to industrial production levels could potentially mitigate this limitation.

3.1.1. XRD analysis of mHA, HA, mHA@thymol, and thymol

The XRD patterns for mHA, HA, mHA@thymol, and thymol are presented in Fig. 1(a–d).

Distinctive peaks for mHA at 2θ values of 25.94° (002), 32.09° (211), 46.54° (222), 49.84° (213), 53.24° (004) and characteristic peaks HA at 26.19° (002), 32.19° (211), 46.99° (222), 49.84° (213) and 53.49° (004) were congruent with the standard crystalline hexagonal HA (JCPDS 01-086-0740) [30,31].

Comparative analysis of the XRD patterns of mHA@thymol and mHA XRD patterns indicates prominent peaks of thymol at 2θ values of 8.04, 12,19 with reflection planes (101) and (110), consistent with the standard for thymol (JCPDS 00-011-0705). These findings corroborate the successful loading of thymol onto mHA. The XRD analysis reveals that mHA@thymol comprises two phases: one is in alignment with the standard of HA (JCPDS Card NO. 00-024-0033), and the other is congruent with thymol (JCPDS Card NO. 00-011-0705). Interestingly, while the thymol patterns closely resemble the highly crystalline standard thymol (JCPDS 00-011-0705), the broader reflections detected in the mHA@thymol XRD spectra suggest an amorphous HA phase. These subtle reflections in the XRD patterns indicate an amorphous transformation of thymol post-loading onto the mesoporous structure of HA [32,33].

3.1.2. FTIR spectra of mHA, HA, mHA@thymol, and thymol

The FTIR spectra for thymol, mHA@thymol, mHA, and HA are depicted in Fig. 2a. Both mHA and HA exhibited characteristic peaks of hydroxyapatite with absorbance bands of PO_4^{-3} observed at 566, 601, 964, and 1031-1095 cm^{-1}. A trace peak at 472 cm^{-1} corresponds to the v_3 bending vibration, while a weak peak for CO_3^{-2} is evident at 1446 cm^{-1}. The band at 3575 cm^{-1} is attributed to OH^{-1}, and the broadband spanning 3000–3450 cm^{-1} describes O–H stretching vibration; water-associated hydrogen bands and bending vibration are also identified at 1631 cm^{-1} [34,35].

In the thymol spectrum, peaks at 734 cm^{-1}, 806 cm^{-1}, 1419 cm^{-1}, 1587 cm^{-1} and 1623 cm^{-1} correspond to C–H bending vibration, out of the plane methylene and phenolic ring C–H and C═C stretching in the benzene ring, respectively (Fig. 2a). Bands between 2863 cm^{-1} and 2962 cm^{-1} signify CH_2 symmetric and asymmetric stretching vibrations, and a peak between 3251 and 3313 cm^{-1} is associate with phenolic OH stretching vibrations, inclusive of hydrogen bonding. Furthermore, the band at 1712 cm^{-1} indicates C–O stretching vibrations in the phenolic group [22].

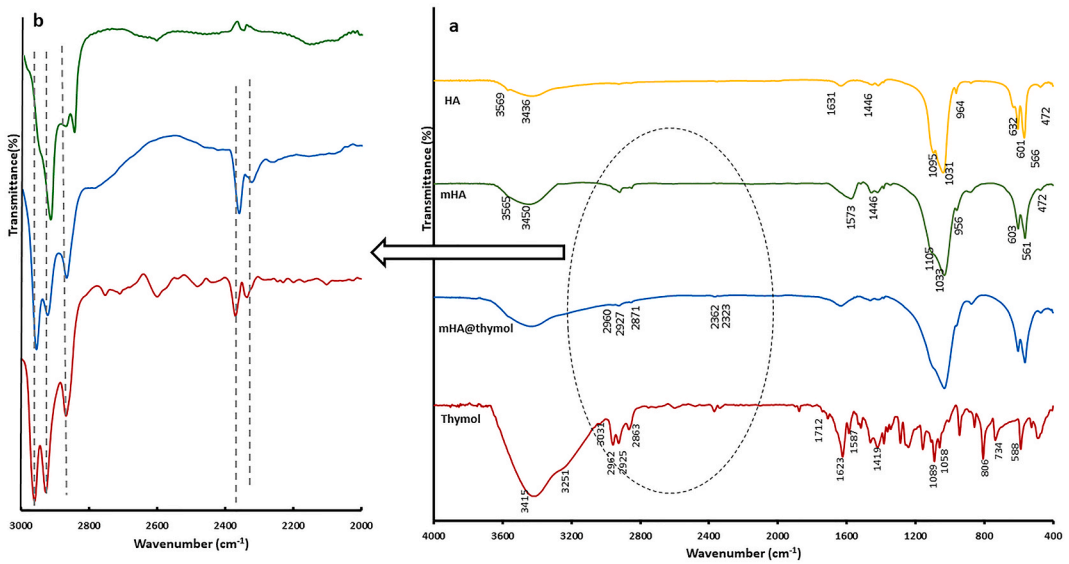

Fig. 2. Fourier Transform Infrared (FTIR) spectra: a) Full spectra range from 400 to 4000 cm^{-1} for HA, mHA, thymol and mHA@thymol; b) Enlarged view of the 2000-3000 cm^{-1} region for mHA, thymol and mHA@thymol.
HA: hydroxyapatite; mHA: mesoporous hydroxyapatite; mHA@thymol: thymol-loaded mHA.

The incorporation of thymol into mHA is further corroborated by FTIR analysis. Bands manifesting at 2871 cm^{-1}, 2927 cm^{-1}, and 2960 cm^{-1} in the mHA@thymol FTIR spectrum are indicative of the symmetric and asymmetric vibration of CH_2 in thymol. An enlarged view of these characteristic bands is presented in Fig. 2b. A noticeable shift from 2867 cm^{-1} to 2871 cm^{-1} upon thymol loading validates the interaction between the hydroxyl group in thymol and HA [23,36]. Moreover, characteristic Orton peaks for thymol appear at 2368 cm^{-1} and 2337 cm^{-1} in the mHA@thymol, with shifts to 2362 cm^{-1} and 2323 cm^{-1}, further confirming the thymol loading onto mHA nanoparticles.

3.1.3. FESEM and EDX analysis

EDX analysis (Fig. 3) showed that the specimen of mHA is primarily composed of Ca, P, and O elements. The resultant Ca/P ratio for mHA powder was determined to be 1.34 through EDX, falling within the synthetic HA Ca/P ratio range of 1.25–2.10 [37].

FESEM micrographs displayed in Fig. 4 correspond to HA (Fig. 4a_1 to a_4), mHA (Fig. 4b_1 to b_4), and mHA@thymol (Fig. 4c_1 to c_4). Four levels of magnifications for each sample -ranging from 8.00 k to 150.00 k-were included. These micrographs exhibit rod and flake-like morphologies alongside instances of agglomeration [38]. Noteworthy is the detection of a porous structure in both mHA and mHA@thymol FESEM images [25]. Fig. 4 (a_1, b_1, and c_1) marks both intraparticle and interparticle pores, underscoring the capacity of these porous materials for high drug adsorption.

3.1.4. DLS analysis

The DLS-based size distribution reveals that the average diameter of mHA and HA are 766.6 and 546.8 nm, respectively. A uniform size distribution between 500 and 800 nm was observed for both materials, as evidenced by DLS analysis (Fig. 5a and b). Notably, these DLS results show a larger diameter than the FESEM micrographs; this discrepancy is attributed to particle aggregation upon sample dispersion in water [13].

3.1.5. N_2 adsorption–desorption measurements

Fig. 6 presents the nitrogen adsorption/desorption isotherms (Fig. 6a_1 and a_2), pore size distributions (Fig. 6b_1 and b_2), and BET-plots (Fig. 6c_1 and c_2) for both mHA and HA. According to the International Union of Pure and Applied Chemistry (IUPAC) classifications, the isotherm of mHA is classified as a type IV isotherm with an H1-hysteresis loop, indicative of mesoporous materials. Conversely, HA exhibits a type V with an H3-hysteresis loop [39]. Pore size distribution analyzed using the BJH model revealed that mHA particle pore sizes range between 2.4 and 51 nm, indicating the presence of mesopores (2–50 nm). In contrast, HA comprises a broader spectrum of pore sizes ranging from 1 nm to 100 nm, encompassing mesopores, macropores, and micropores regarding IUPAC classification [8,39]. A greater pore volume of 0.74 $cm^3\ g^{-1}$ was observed for mHA, as listed in Table 2. The BET surface areas were calculated as 167.1 m^2/g for mHA and 62.7 m^2/g for HA. Previously, Munir et al. had synthesized hollow mesoporous hydroxyapatite nanoparticles (hmHANPs) with 105.33 $m^2\ g^{-1}$ specific surface area and 0.533 $cm^3\ g^{-1}$ pore volume [30]. Safi et al. also reported that synthesized mHA had an 85 $m^2\ g^{-1}$ surface area and 0.4227 $cm^3\ g^{-1}$ pore volume [25]. The present study's findings indicate a larger surface area and greater pore volume for synthesized mHA compared to previous reports, which depict mHA as an excellent adsorbent [8,40]. Both BET and BJH analyses confirm the porous nature observed in FESEM micrographs.

3.1.6. Thymol loading

Thymol adsorption onto mHA and HA was evaluated by plotting the adsorption capacity -quantity of thymol adsorbed per unit mass of the adsorbent (μg mg^{-1})- against contact time as shown in Fig. 7. Thymol adsorption was quantified following Equation (1). The study involved immersing varying amounts of mHA in different thymol concentrations, as detailed in Section 2.3. Maximum adsorption was observed at an elevated liquid-to-solid ratio, approximately 162.574 μg mg^{-1} (~77.83 % of thymol adsorbed onto

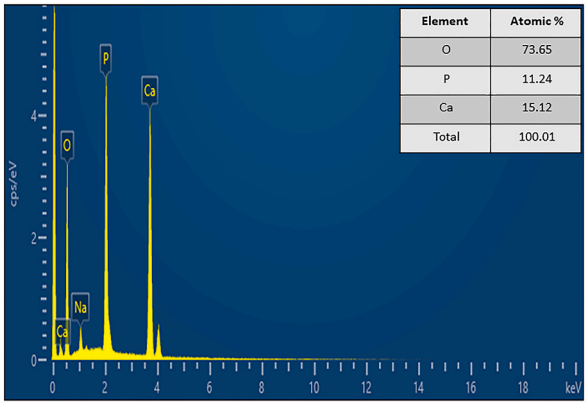

Fig. 3. Elemental composition of mHA determined by Energy-Dispersive X-ray (EDX) analysis.
mHA: mesoporous hydroxyapatite.

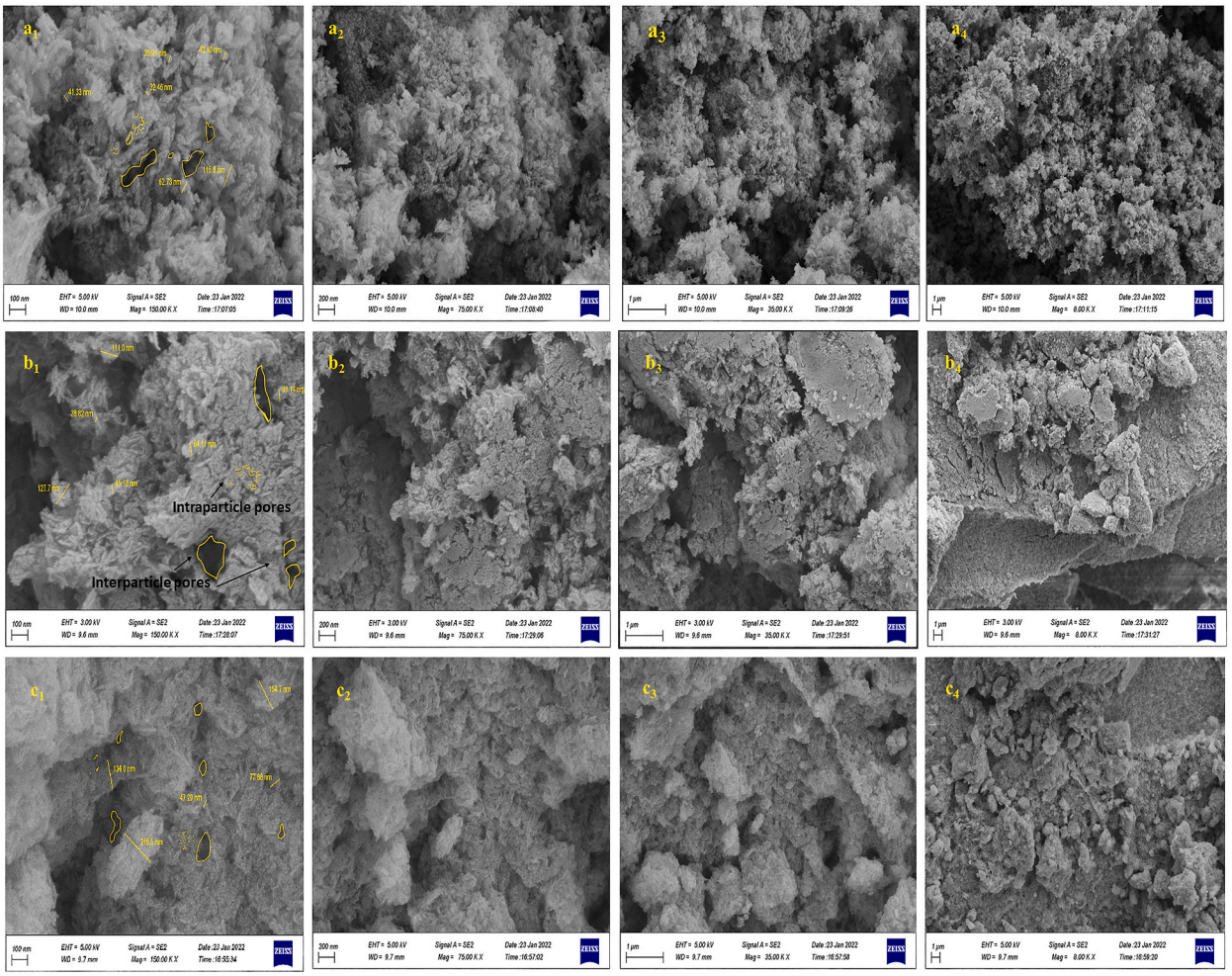

Fig. 4. Field Emission Scanning Electron Microscopy (FESEM) images of a_1 to a_4) HA, b_1 to b_4) mHA, and c_1 to c_4) mHA@thymol at various magnification (8.00 kx, 35.00 kx, 75.00 kx, 150.00 kx).
HA: hydroxyapatite; mHA: mesoporous hydroxyapatite; mHA@thymol: thymol-loaded mHA.

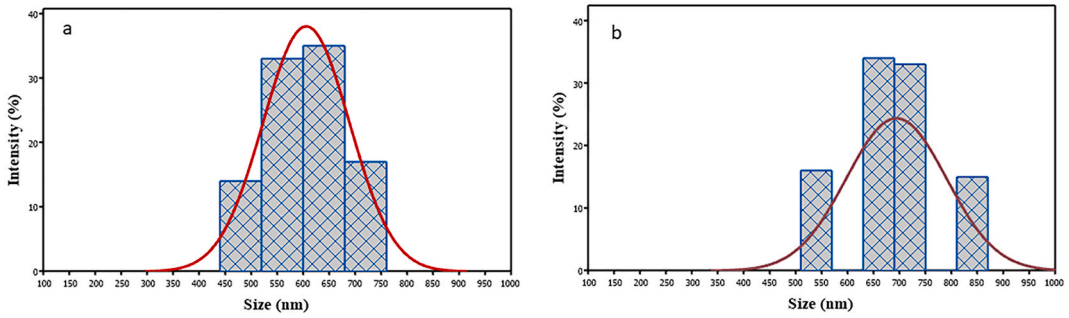

Fig. 5. Dynamic Light Scattering (DLS) particle size distributions of a) HA b) mHA. HA: hydroxyapatite; mHA: mesoporous hydroxyapatite.

mHA), as presented in Fig. 7a. A similar trend was evident for HA, with maximum thymol adsorption measured at 166.574 μg mg^{-1} (Fig. 7b). These results affirm a strong binding affinity of thymol to both mHA and HA [41,42].

3.1.7. Thymol release

Fig. 8 illustrates the cumulative release profiles of thymol from the thymol solution (control), mHA@thymol, and HA@thymol. Thymol release was quantified using UV-VIS at a wavelength of 276. Comparative analyses of the release profiles of mHA@thymol and

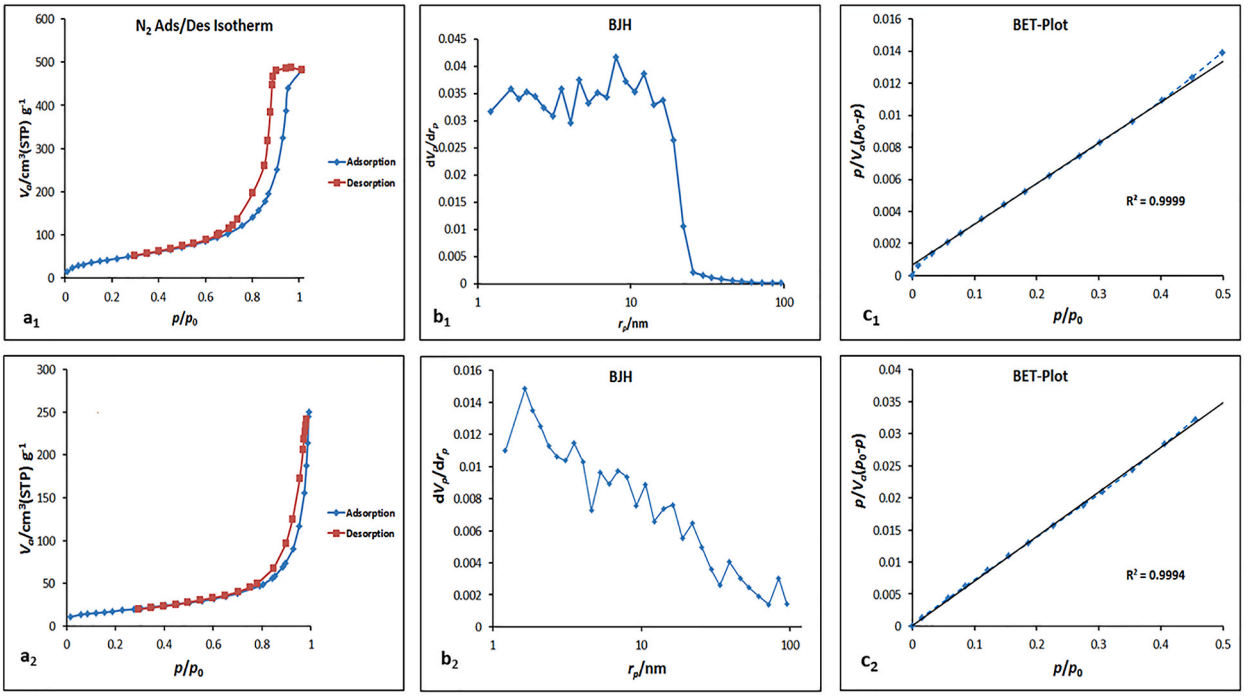

Fig. 6. N_2 adsorption-desorption isotherms measured at 77 °k (a_1 and a_2); pore size distribution curves (b_1 and b_2) and Brunauer-Emmett-Teller (BET) plots (c_1 and c_2) of mHA and HA, respectively. mHA: mesoporous hydroxyapatite; HA: hydroxyapatite.

Table 2
Surface area characteristic of mHA and HHA assessed via Brunauer-Emmett-Teller (BET) and Barrett-Joyner-Halenda (BJH) methods.

Sample	BET				BJH		
	V_m (Ml/g)	$a_{s,BET}$ (m^2/g)	V_{tot} (Ml/g)	d_p (nm)	V_p (Ml/g)	r_p (nm)	a_p (m^2/g)
mHA	38.4	167.1	0.72	17.3	0.74	8.0	217.5
HA	14.4	62.7	0.38	24.4	0.38	1.6	71.2

mHA, mesoporous hydroxyapatite; HA, hydroxyapatite; V_m, volume of gas adsorbed at Standard Temperature and Pressure (STP); a_s, BET surface area; V_{tot}, total pore volumes measured at ($p/p_0 = 0.990$); d_p, mean pore diameter; V_p, mean volume of the pores; r_p, radius of pores; a_p, surface of pores.

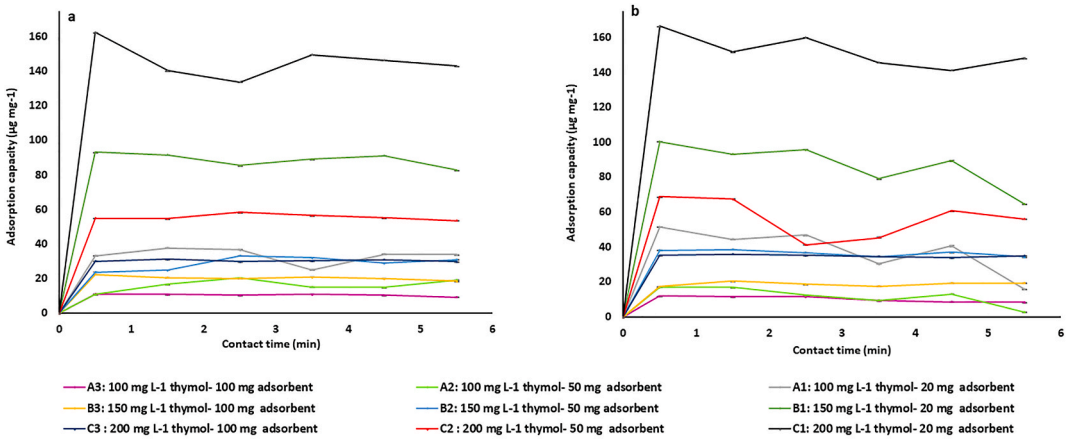

Fig. 7. Adsorption capacity of a) mHA b) HA under varying initial thymol concentrations and contact times at 20, 50, 100 mg doses of mHA and HA. mHA: mesoporous hydroxyapatite; HA: hydroxyapatite.

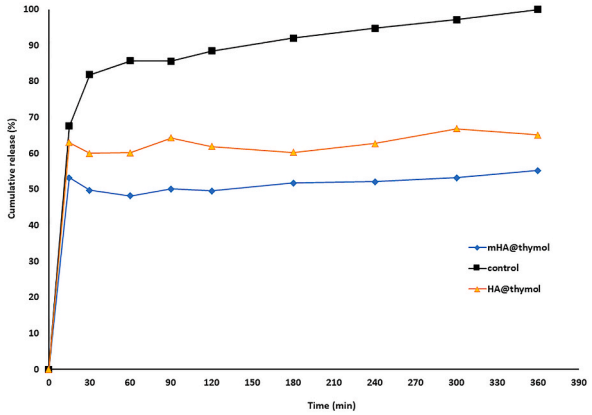

Fig. 8. Percentage of cumulative thymol release from mHA@thymol, HA@thymol, and control* formulations in a Franz diffusion cell through a cellulose membrane, at 37° C over a 6-h period.
HA@thymol: thymol-loaded mHA; HA@thymol: thymol-loaded HA.
*Control = thymol solution.

Table 3
Similarity factors (f_2) of thymol release profile between mHA@thymol-Control*, HA@thymol-control, mHA@thymol-HA@thymol, as determined by UV–visible spectroscopy.

Test-Reference	f_2
mHA@thymol-Control	24.49
HA@thymol-Control	28.54
HA@thymol- mHA@thymol	47.13

mHA@thymol, thymol-loaded mHA; HA@thymol, thymol loaded HA. *control = thymol Solution.

HA@thymol revealed statistically significant differences, as evidenced by a f_2 value of less than 50. Similar significant differences were also found when comparing the profiles to the control (Table 3). These observed differences are ascribed to the mesoporous structure, tunable pore size, and large surface area of mHA, which aligns with findings from previous studies [43,44]. A rapid initial release of thymol was detected 15 min into the experiment for both mHA and HA, with 53.3 % and 63 % release, respectively. This timeframe marked the greatest disparity in thymol release rates between mHA@thymol and HA@thymol. Beyond this initial period, the release profiles attained equilibrium. The initial release likely corresponds to the desorption of drug molecules from the adsorbents' exterior surfaces, followed by a more extended desorption period from the interior pores. Compared to the control, approximately 55 % of thymol was released from mHA and 65 % from HA over 6 h. These results are consistent with controlled release systems reported in existing literature [25,34,36].

3.2. Evaluation of toothpaste

Toothpaste formulations were developed, incorporating varying types of abrasive, including mHA in the first formulation and HA in the second. All ingredients should be judiciously chosen, as they significantly influence the quality of the final formulation. Carbopol, HPMC, and CMC Na were utilized as thickening and binding agents, adding viscosity and smoothness to the paste. Sorbitol and glycerin were used as humectants, maintaining moisture and inhibiting dryness, while SLS was used as foaming agent. Sodium saccharin and peppermint oil acted as sweetening and flavoring agents, effectively masking the bitter flavor of other constituents [28].

3.2.1. Physical stability and organoleptic properties

The formulated toothpaste demonstrated long-term physical stability over a one-year screening period, showing consistency in uniformity, smoothness, color, and taste at room temperature without any phase separation. Based on these findings, long-term stability appears highly likely. Previous studies corroborate these stability outcomes, with one research showcasing favorable formulation stability in toothpaste containing *T. vulgaris* essential oil [45] and another indicating robust stability in HA-based dentifrice [46]. Both mHA and HA toothpaste exhibited appropriate organoleptic and physical properties (as summarized in Table 4), aligning with existing literature [45,47].

Enhanced palatability and olfactory qualities were noted for the mHA-based formulation, likely due to the mesoporous structure's capacity to mask the intense flavor and odor of thymol [23].

Table 4
Assessment of organoleptic and physical Properties of mHA and HA toothpaste formulations.

Formulation number/Parameters	Uniformity	Smoothness	Taste	Odor	Color	Spreadability	Dryness
F_1(mHA)	+++	++	+++	+++	**W**	+++	-
F_2(HA)	++	++	++	++	**W**	++	-

'-': Not acceptable, '+': partially acceptable, '++': acceptable; '+++': very acceptable; 'w': white.

Table 5
Comparative analysis of enamel and dentin roughness: Evaluation of formulated toothpastes against a standard toothpaste reference.

Group	Enamel roughness (μm) Mean ± SD	P value	Roughness compared to standard (times)	Dentine roughness (μm) Mean ± SD	Roughness compared to standard (times)	P value
Standard	0.480 ± 0.360		–	0.491 ± 0.210	–	
F_1 (mHA)	0.307 ± 0.125	0.475	0.64	0.331 ± 0.113	0.67	0.309
F_2(HA)	0.210 ± 0.082	0.247	0.44	0.208 ± 0.098	0.42	0.101

3.2.2. pH assessment

The pH clues of mHA and HA-based formulations containing thymol were 7.1 and 7.2, respectively. The results reveal that the pH is in the standard range according to ISO11609 [29].

3.2.3. Toothpaste abrasiveness on enamel and dentin

The abrasiveness of mHA and HA toothpastes on dentin were 0.67 and 0.42, and on enamel were 0.64 and 0.44 times compared to reference toothpaste, respectively (Table 5). Independent sample t-tests did not reveal statistically significant differences between the profilometric means before and after enamel and dentine abrasion by both formulations compared to standard toothpaste ($p = 0.475$, 0.274, 0.309, and 0.101, respectively). This suggested that both mHA and HA toothpastes exhibit acceptable abrasive characteristics, which is consistent with previous reports [45,48].

4. Conclusion

The Specific surface area in mHA is markedly greater than in HA, making it the principal factor contributing to the enhanced adsorption efficiency observed in these structures. Based on the experimental outcomes, the mesoporous structure of mHA is likely accountable for its enhanced abrasive characteristics, thereby improving its cleaning efficacy. Furthermore, the unique mesoporous and hollow structural attributes position mHA as an effective carrier for delivering active agents within the oral cavity. Overall, mHA emerges as a promising candidate for the design of toothpaste formulations, offering multifaced benefits. However, further investigation is warranted to substantiate its clinical effectiveness. Additionally, future research must focus on synthesizing mHA on an industrial scale, which is essential for developing diverse formulations suitable for clinical studies.

Data availability

Researchers interested in more in-depth information or additional data relating to any segment of the current study are encouraged to contact the corresponding author. We are readily willing to furnish any requested data to contribute to the advancement of scientific understanding in this field.

Ethical Considerations

While the current study does not fall under clinical trials or pre-clinical assessments and did not involve testing on human or animal populations for therapeutic efficacy, ethical considerations were rigorously adhered to in the only section involving human participation, i.e., the organoleptic assessment phase of the research. In compliance with ethical guidelines, all volunteers were thoroughly briefed about the scope of the study, the formulations being assessed, and the parameters being examined. Before participating, each volunteer provided written informed consent, affirming their understanding of the study and willingness to participate under the outlined conditions.

CRediT authorship contribution statement

Azarmidokht Nikfallah: Investigation, Methodology, Writing – original draft, Writing – review & editing. **Ali Mohammadi:** Formal analysis, Methodology, Supervision, Visualization, Writing – original draft. **Mohammadsadegh Ahmadakhondi:** Data curation, Formal analysis, Supervision, Writing – original draft. **Mehdi Ansari:** Dogaheh, Conceptualization, Data curation, Formal analysis, Investigation, Methodology, Project administration, Resources, Supervision, Validation, Visualization, Writing – original draft, Writing – review & editing.

Declaration of competing interest

The authors declare that they have no known competing financial interests or personal relationships that could have appeared to influence the work reported in this paper.

References

[1] T. Mangilal, M. Ravikumar, Preparation and evaluation of herbal toothpaste and compared with commercial herbal toothpastes: an in vitro study, Int. J. Ayurvedic Herb. Med. 6 (2016) 2266–2273.
[2] P. Zampetti, A. Scribante, Historical and bibliometric notes on the use of fluoride in caries prevention, Eur. J. Paediatr. Dent. 21 (2020) 148–152, https://doi.org/10.23804/ejpd.2020.21.02.10.
[3] S. Demir, G. Keskin, N. Akal, Y. Zer, Antimicrobial effect of natural kinds of toothpaste on oral pathogenic bacteria, J. Infect. Dev. Ctries. 15 (2021) 1436–1442, https://doi.org/10.3855/jidc.14966.
[4] M.G. Singla, I. Virdi, Abrasive action of different herbal toothpastes: a profilometric analysis, J. Dent. Res. Rev. 8 (2021) 312–316, https://doi.org/10.4103/jdrr.jdrr_96_21.
[5] S. Ali, I. Farooq, F. Shahid, U. Hassan, M.S. Zafar, Common toothpastes abrasives and methods of evaluating their abrasivity, J. Oral Res. (2020) 9–15, https://doi.org/10.17126/joralres.2020.055.
[6] N. Jamwal, A. Rao, R. Shenoy, M. Pai, K. Aparna, B. Avinash, Effect of whitening toothpaste on surface roughness and microhardness of human teeth: a systematic review and meta-analysis. https://doi.org/10.12688/f1000research.76180.3, 2022. F1000Res, 11.
[7] D. Kumari, V. Tandon, D. Medhi, D. Sharma, Comparative evaluation of tooth surface abrasiveness of herbal and non-herbal toothpaste, Clin. Dent. 16 (2022) 12–15, https://doi.org/10.21276//ujds.2023.9.2.3, 0974-3979.
[8] W. Wijesinghe, M. Mantilaka, T.N. Peiris, R. Rajapakse, K.U. Wijayantha, H. Pitawala, T. Premachandra, H. Herath, R. Rajapakse, Preparation and characterization of mesoporous hydroxyapatite with non-cytotoxicity and heavy metal adsorption capacity, New J. Chem. 42 (2018) 10271–10278, https://doi.org/10.1039/C8NJ00673C.
[9] L. Chen, S. Al-Bayatee, Z. Khurshid, A. Shavandi, P. Brunton, J. Ratnayake, Hydroxyapatite in oral care products—a review, Materials 14 (2021) 4865, https://doi.org/10.3390/ma14174865.
[10] A. Butera, M. Pascadopoli, M. Pellegrini, B. Trapani, S. Gallo, M. Radu, A. Scribante, Biomimetic hydroxyapatite paste for molar–incisor hypomineralization: a randomized clinical trial, Oral Dis. (2022), https://doi.org/10.1111/odi.14388.
[11] A. Anil, W.I. Ibraheem, A.A. Meshni, R.S. Preethanath, S. Anil, Nano-hydroxyapatite (nHAp) in the remineralization of early dental caries: a scoping review, Int. J. Environ. Res. Public Health. 19 (2022) 5629, https://doi.org/10.3390/ijerph19095629.
[12] T. Habibah, D. Amlani, M.S. Brizuela, Hydroxyapatite dental material, in: Statpearls, StatPearls Publishing, Treasure Island, FL, USA, 2020.
[13] K. Ma, H. Cui, A. Zhou, H. Wu, X. Dong, F. Zu, J. Yi, R. Wang, Q. Xu, Mesoporous hydroxyapatite: synthesis in molecular self-assembly and adsorption properties, Microporous Mesoporous Mater. 323 (2021), 111164, https://doi.org/10.1016/j.micromeso.2021.111164.
[14] B. Siddiqui, A.A. Al-Dossary, A. Elaissari, N. Ahmed, Exploiting recent trends for the synthesis and surface functionalization of mesoporous silica nanoparticles towards biomedical applications, Int. J. Pharm. X (2022), 100116, https://doi.org/10.1016/j.ijpx.2022.100116.
[15] M.U. Munir, S. Salman, A. Ihsan, T. Elsaman, Synthesis, characterization, functionalization and bio-applications of hydroxyapatite nanomaterials: an overview, Int. J. Nanomed. 17 (2022) 1903–1925, https://doi.org/10.2147/IJN.S360670.
[16] U. Erdem, M. Dogan, A.U. Metin, S. Baglar, M.B. Turkoz, M. Turk, S. Nezir, Hydroxyapatite-based nanoparticles as a coating material for the dentine surface: an antibacterial and toxicological effect, Ceram. Int. 46 (2020) 270–280, https://doi.org/10.1016/j.ceramint.2019.08.260.
[17] K. Singh, P. Singh, G. Oberoi, Comparative studies between herbal toothpaste (dantkanti) and nonherbal Toothpaste, Int. J. Dent. Res. 4 (2016) 53–56, https://doi.org/10.14419/ijdr.v4i2.6633.
[18] A. Escobar, M. Perez, G. Romanelli, G. Blustein, Thymol bioactivity: a review focusing on practical applications, Arab. J. Chem. 13 (2020) 9243–9269, https://doi.org/10.1016/j.arabjc.2020.11.009.
[19] D. Sahin, B. Saka, Development of antibacterial toothpaste formulation using natural raw materials, TOJSAT 11 (2021) 66–70.
[20] V.C. Patole, S.P. Chaudhari, Development of thymol microsponges loaded in situ gel for the treatment of periodontitis, Curr. Drug Deliv. 18 (2021) 71–87, https://doi.org/10.2174/1567201817666200804111614.
[21] Y. Chen, Y. Qiu, W. Chen, Q. Wei, Electrospun thymol-loaded porous cellulose acetate fibers with potential biomedical applications, Mater. Sci. Eng. C 109 (2020), 110536, https://doi.org/10.1016/j.msec.2019.110536.
[22] M. Shahriarinour, F. Divsar, Z. Eskandari, Synthesis, characterization, and antibacterial activity of thymol loaded SBA-15 mesoporous silica nanoparticles, Inorg. Nano-Met. Chem. 49 (2019) 182–189, https://doi.org/10.1080/24701556.2019.1624569.
[23] Y. Liu, L. Jin, C. Wang, J. Sheng, Y. Song, Thymol-functionalized hollow mesoporous silica spheres nanoparticles: preparation, characterization and bactericidal activity, Bull. Mater. Sci. 44 (2021) 1–7, https://doi.org/10.1007/s12034-021-02425-2.
[24] R.M. Abdelhameed, E. Alzahrani, A.A. Shaltout, H.E. Emam, Temperature-controlled-release of essential oil via reusable mesoporous composite of microcrystalline cellulose and zeolitic imidazole frameworks, J. Ind. Eng. Chem. 94 (2021) 134–144, https://doi.org/10.1016/j.jiec.2020.10.025.
[25] S. Safi, F. Karimzadeh, S. Labbaf, Mesoporous and hollow hydroxyapatite nanostructured particles as a drug delivery vehicle for the local release of ibuprofen, Mater. Sci. Eng. C 92 (2018) 712–719, https://doi.org/10.1016/j.msec.2018.07.004.
[26] J. Moore, H. Flanner, Mathematical comparison of dissolution profiles, Pharm. Technol. 20 (1996) 64–75.
[27] M. Botelho, N. Nogueira, G. Bastos, S. Fonseca, T. Lemos, F. Matos, D. Montenegro, J. Heukelbach, V. Rao, G. Brito, Antimicrobial activity of the essential oil from Lippia sidoides, carvacrol and thymol against oral pathogens, Braz. J. Med. Biol. 40 (2007) 349–356, https://doi.org/10.1590/S0100-879X2007000300010.
[28] G. Sharma, J. Gadiya, M. Dhanawat, Textbook of Cosmetic Formulations, Department of Pharmacy, Mewar University, 2018, p. 901. Rajasthan-312.
[29] ISO 11609:2017(E); Dentistry—Dentifrices—Requirements, Test Methods and Making, third ed., International Standardization Organization, Geneva, Switzerland, 2017.
[30] M.U. Munir, A. Ihsan, Y. Sarwar, S.Z. Bajwa, K. Bano, B. Tehseen, N. Zeb, I. Hussain, M.T. Ansari, M. Saeed, Hollow mesoporous hydroxyapatite nanostructures; smart nanocarriers with high drug loading and controlled releasing features, Int. J. Pharm. 544 (2018) 112–120, https://doi.org/10.1016/j.ijpharm.2018.04.029.
[31] J.A. Lett, S. Sagadevan, J.J. Prabhakar, N.A. Hamizi, I.A. Badruddin, M.R. Johan, A.R. Marlinda, Y. Abdul Wahab, T.M. Yunus Khan, S. Kamangar, Drug leaching properties of Vancomycin loaded mesoporous hydroxyapatite as bone substitutes, Processes 7 (2019) 826, https://doi.org/10.3390/pr7110826.
[32] E. Juère, F. Kleitz, On the nanopore confinement of therapeutic drugs into mesoporous silica materials and its implications, Microporous Mesoporous Mater. 270 (2018) 109–119, https://doi.org/10.1016/j.micromeso.2018.04.031.
[33] W. Zhou, Y. Zhang, R. Li, S. Peng, R. Ruan, J. Li, W. Liu, Fabrication of caseinate stabilized thymol nanosuspensions via the ph-driven method: enhancement in water solubility of thymol, Foods 10 (2021) 1074, https://doi.org/10.3390/foods10051074.
[34] N.A. Aval, J.P. Islamian, M. Hatamian, M. Arabfirouzjaei, J. Javadpour, M.-R. Rashidi, Doxorubicin loaded large-pore mesoporous hydroxyapatite coated superparamagnetic Fe3O4 nanoparticles for cancer treatment, Int. J. Pharm. 509 (2016) 159–167, https://doi.org/10.1016/j.ijpharm.2016.05.046.
[35] J. Chen, J. Liu, H. Deng, S. Yao, Y. Wang, Regulatory synthesis and characterization of hydroxyapatite nanocrystals by a microwave-assisted hydrothermal method, Ceram. Int. 46 (2020) 2185–2193, https://doi.org/10.1016/j.ceramint.2019.09.203.

[36] E. Gámez, H. Elizondo-Castillo, J. Tascon, S. García-Salinas, N. Navascues, G. Mendoza, M. Arruebo, S. Irusta, Antibacterial effect of thymol loaded SBA-15 nanorods incorporated in PCL electrospun fibers, Nanomaterials 10 (2020) 616, https://doi.org/10.3390/nano10040616.
[37] M.V. Chaikina, N.V. Bulina, O.B. Vinokurova, K.B. Gerasimov, I.Y. Prosanov, N.B. Kompankov, O.B. Lapina, E.S. Papulovskiy, A.V. Ishchenko, S.V. Makarova, Possibilities of mechanochemical synthesis of apatites with different Ca/P ratios, Ceramics 5 (2022) 404–422, https://doi.org/10.3390/ceramics5030031.
[38] N.M. Pu'ad, P. Koshy, H. Abdullah, M. Idris, T. Lee, Syntheses of hydroxyapatite from natural sources, Heliyon 5 (2019), e01588, https://doi.org/10.1016/j.heliyon.2019.e01588.
[39] M. Thommes, K. Kaneko, A.V. Neimark, J.P. Olivier, F. Rodriguez-Reinoso, J. Rouquerol, K.S. Sing, Physisorption of gases, with special reference to the evaluation of surface area and pore size distribution (IUPAC Technical Report), Pure Appl. Chem. 87 (2015) 1051–1069, https://doi.org/10.1515/pac-2014-1117.
[40] M. Liu, F. Huang, C.-T. Hung, L. Wang, W. Bi, Y. Liu, W. Li, An implantable antibacterial drug-carrier: mesoporous silica coatings with size-tunable vertical mesochannels, Nano Res. 15 (2022) 4243–4250, https://doi.org/10.1007/s12274-021-4055-y.
[41] N. Hasani, T. Selimi, A. Mele, V. Thaçi, J. Halili, A. Berisha, M. Sadiku, Theoretical, equilibrium, kinetics and thermodynamic investigations of methylene blue adsorption onto lignite coal, Molecules 27 (2022) 1856, https://doi.org/10.3390/molecules27061856.
[42] K. Sharma, S. Sharma, V. Sharma, P.K. Mishra, A. Ekielski, V. Sharma, V. Kumar, Methylene blue dye adsorption from wastewater using hydroxyapatite/gold nanocomposite: kinetic and thermodynamics studies, Nanomaterials 11 (2021) 1403, https://doi.org/10.3390/nano11061403.
[43] R.P. Singh, A.S. Kang, Novel morphologies of mesoporous hierarchically assembled nanostructured hydroxyapatite particles: influence of some synthesis conditions, Ceram. Int. (2022), https://doi.org/10.1016/j.ceramint.2022.07.027.
[44] M. Šoltys, D. Zůza, T. Boleslavská, S.M. Akhlasová, M. Balouch, P. Kovačík, J. Beranek, N. Škalko-Basnet, G.E. Flaten, F. Štěpánek, Drug loading to mesoporous silica carriers by solvent evaporation: a comparative study of amorphization capacity and release kinetics, Int. J. Pharm. 607 (2021), 120982, https://doi.org/10.1016/j.ijpharm.2021.120982.
[45] M. Kiani, F. Firozian, S. Moradkhani, Formulation and physicochemical evaluation of toothpaste formulated with Thymus vulgaris essential oil, J. Herbmed Pharmacol. 6 (2017) 130–135.
[46] R.A. Lucas, A.J. Smith, W. Changxiang, Dentifrice Composition Comprising Sintered Hydroxyapatite, Google Patents, 2016.
[47] O.O. Oluwasina, S.O. Idris, C.O. Ogidi, F.O. Igbe, Production of herbal toothpaste: physical, organoleptic, phyto-compound, and antimicrobial properties, Heliyon 9 (2023), https://doi.org/10.1016/j.heliyon.2023.e13892.
[48] R.S. Alofi, H.A. Alsuayri, L.S. Mohey, A.S. Alofi, Efficiency of activated charcoal powder in stain removal and effect on surface roughness compared to whitening toothpaste in resin composite: in vitro study, Saudi Dent. J. 33 (2021) 1105–1110, https://doi.org/10.1016/j.sdentj.2021.03.010.